Fuel 193 (2017) 31–38

Contents lists available at ScienceDirect

Fuel

journal homepage: www.elsevier.com/locate/fuel

Full Length Article

CFD modeling of combustion of sugarcane bagasse in an industrial boiler

Felipe Orlando Centeno-González [a,b,*], Electo Eduardo Silva Lora [b], Helcio Francisco Villa Nova [b], Lourival Jorge Mendes Neto [b], Arnaldo Martín Martínez Reyes [c], Albert Ratner [d], Mohsen Ghamari [e]

[a] Faculty of Engineering, Universidad de la Costa, Calle 58 N 55-66, Barranquilla, Colombia
[b] The Excellence Group in Thermal Power and Distributed Generation (NEST), Mechanical Engineering Institute, The Federal University of Itajuba, Av. BPS 1303 Pinheirinho, Itajuba, MG, Brazil
[c] University of Oriente, Sede J.A. Mella, Ave. de las Américas s/n y calle I., C.P. 90900 Santiago de Cuba, Cuba
[d] Department of Mechanical and Industrial Engineering, University of Iowa, 3131 SC, Iowa City, IA 52242, USA
[e] Department of Mechanical Engineering, Wilkes University, Wilkes-Barre, PA 18766, USA

ARTICLE INFO

Article history:
Received 1 June 2016
Received in revised form 24 November 2016
Accepted 26 November 2016
Available online 22 December 2016

Keywords:
Computational fluid dynamics
Combustion
Sugarcane bagasse
Boiler

ABSTRACT

In this study, a CFD model is developed to evaluate the performance of an industrial boiler furnace running on sugarcane bagasse. The model was developed in the commercial software ANSYS FLUENT and includes user-defined functions programmed in C language defining devolatilization phenomenon as well as combustion on the grate. The simulation results suggests that devolatilization is the dominant phenomenon through the largest portion of the particle trajectory, and hence an important factor in predicting the thermal fields. On the other hand, the char is burned on the grate or entrained through the furnace outlet. The general efficiency indicators obtained from particle combustion description could then allow us to compare different design and operational alternatives.

1. Introduction

Early developments of CFD modeling for combustion of polydisperse solid fuels are referred to pulverized coal. Since the techniques for modeling coal combustion have been already well developed through quite mature methodologies, it is now possible to find some models available in commercial CFD software. Although these developments have been taken as a basis for applications regarding biomass combustion modeling, CFD modeling techniques in this area are still facing challenges due to significant differences between the burning of polydisperse biomass and pulverized coal.

In comparison with coal, Demirbas [1] and Belosevic [2] pointed out that biomass usually has more oxygen, moisture, silica, potassium, and aluminum and lower fixed carbon content, iron, density, calorific value and friability. According to Bharadwaj et al. [3], biomass particles have considerably lower densities than coal particles, commonly differing by a factor of 4–7. Biomass also has a typically very low sulfur content compared to coal. In addition, the chlorine contents of certain biomass can exceed the levels of coal. According to Belosevic [2] chlorine has a strong influence on ash formation because it facilitates the mobility of many inorganic compounds, in particular potassium. The critical influence of these parameters on the formation of agglomerations and deposits and also the significant differences in organic composition of different biomasses makes it necessary to conduct a particular study of each biomass intended to be used for combustion in boiler furnaces.

In terms of volatility, biomass always has greater volatiles content, even when compared to low-rank coals [2,4]. As stated by Demirbas [1], the relative volatility, i.e. the ratio of volatile matter "MV" to fixed carbon "CF", typically is MV/CF > 4.0 for biomass and MV/CF < 1.0 for coal. In devolatilization modeling, the CFD models have mostly used an Arrhenius single rate model to represent the devolatilization sub-model [5–22]. However, given the importance of devolatilization, which was identified in a sensitivity study by Smith [23] as the largest physical control phenomenon, these single sub-models cannot adequately represent the devolatilization [24]. Another important difference between biomass and coal combustion in boiler furnaces is in their states of combustion; the coal to be burned is first pre-dried and then finely pulverized, helping it to mainly burn in suspension. On the other hand, many polydisperse biomasses are usually wet burned whereby part of biomass is burned on the grate like in a fixed bed.

* Corresponding author at: Faculty of Engineering, Universidad de la Costa (CUC), Calle 58 N 55-66, Barranquilla, Colombia.
E-mail addresses: fcenteno1@cuc.edu.co, fcenteno@ingenieros.com (F.O. Centeno-González).

http://dx.doi.org/10.1016/j.fuel.2016.11.105
0016-2361/

Table 1
Parameters for porous medium replacing the grate in the model.

	Inertial resistance (1/m)	Viscous resistance ($1/m^2$)
Direction 1 (−0.103, 0.994, 0)	4.5145×10^5	3.3086×10^8
Direction 2 (0, 0, 1)	4.5145×10^8	3.3086×10^{11}
Direction 3 (0.994, 0.103, 0)	4.5145×10^8	3.3086×10^{11}

According to recent data by Food and Agriculture Organization of the United Nation (FAO), Brazil is by far the largest producer of sugarcane in the world by producing more than 730 million tons in 2014 [25]. The abundance of sugarcane in Brazil is a consequence of a huge ethanol production industry [26]; this ethanol has a very high net energy balance (defined as the ratio of the energy contained in a given volume of ethanol divided by the fossil energy required for its production) compared to the alcohol made from other crops and so currently more than 90% of all vehicle sales in Brazil are dual fuels and can run on sugarcane ethanol [27]. However, when it comes to the production of steam and electricity, many technical-economic and life cycle assessment studies have shown that yet the best option for utilizing sugarcane bagasse remains to be its direct combustion in furnace [28–36]. While experimental research in this area comes with many complications in terms of logistics, cost, emission and required time for measurements, numerical analysis could provide thoughtful data on different iterations in a timely manner and with minimum cost.

To study the combustion of sugarcane bagasse in an industrial boiler, this paper presents a CFD model developed in commercial software ANSYS FLUENT 15.0 in conjunction with User Defined Functions (UDFs) programmed in C language developed for both devolatilization and grate combustion phenomena. Both physical and gasification properties of bagasse are obtained from experimental measurements and incorporated into the model. Finally, the thermal field and combustion behavior inside the boiler are predicted and several integral performance indicators are obtained.

2. Physical models

All of the simulations were performed in commercial software ANSYS FLUENT R15.0. The modeled case is a "non-premixed combustion", wherein the biomass and air enter the reaction zone through different streams. The model assumes a continuous phase of reacting gases and a discrete phase of fuel particles setting the positions of the mass and heat sources while they travel immersed in the continuous phase.

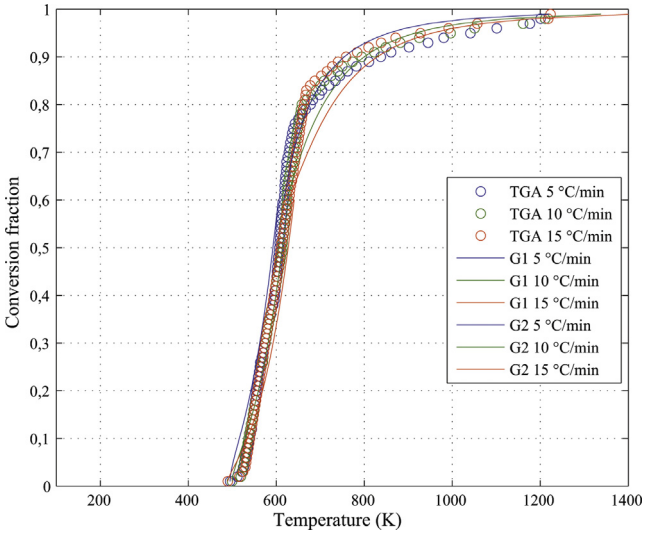

Fig. 1. Thermogram and devolatilization model adjusted using OFW.

Table 3
Kinetic data of release of volatile.

Conversion fraction interval	$0.0 \leqslant \alpha \leqslant 0.6$	$0.6 < \alpha \leqslant 1.0$
A_i (s^{-1}]	88655.18	64561.73
E_{ai} (J/mol)	65173.70	60898.02
$f(\alpha)$	Second order	Third order
Equation	(2)	(3)

2.1. Continuous phase

The continuous phase is a gas mixture, consisting of six species (volatiles, oxygen, carbon dioxide, water vapor, carbon monoxide and nitrogen), whose composition is determined by solving the mass conservation equation, as well as species conservation equations for five of the six species, except nitrogen which is calculated by difference. Since the furnace operates at a constant atmospheric pressure, the density of the gas changes only as a function of temperature and so the state equation for incompressible ideal gases could be employed.

Once the phenomenon can be categorized as non-premixed combustion, where the fuel and the oxidant enter into the reaction zone at different streams, the effects of turbulence on the reaction rate should also be considered. Since in our nonpremixed system the turbulence slowly mixes cold reactants and hot products into the reaction zone, where reaction occurs rapidly, the Eddy-Dissipation Model for species transport is used.

Table 2
Models used in the furnace simulation.

Phase	Models		Section in the Supplementary Material
Continuous phase (Eulerian approach)	Gas mixture	Continuity equation	A.1
		Momentum equation	A.2
		Energy equation	A.3
		Turbulence by k-epsilon standard	A.5
		Radiation by discrete ordinates	A.4
		Equation of state for incompressible ideal gases	A.6
		Species transport by eddy-dissipation model	A.7
	Grate	Momentum equation for porous-media	A.8
		Full burning (UDF)	See UDFs as Supplementary Material
Discrete phase (Lagrangian approach)	Particle motion	Particle forces balance	A.9
	Heat and mass exchange	Inert heating or Cooling	A.10
		Drying (vaporization and boiling)	A.11 and A.12
		Devolatilization (UDF)	See Eqs. (2), (3) and UDFs as Supplementary Material
		Char combustion	A.13

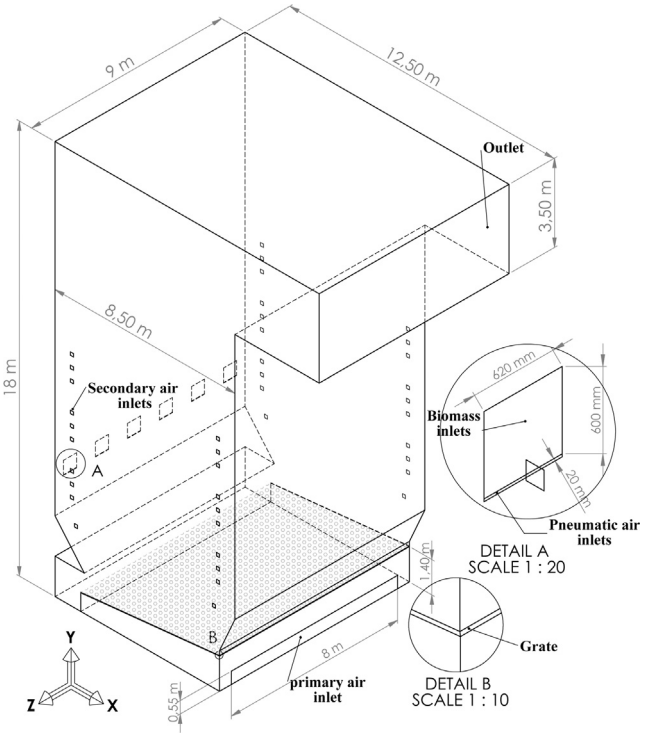

Fig. 2. Furnace geometry characteristics.

Table 4
Proximate analysis of the sugarcane bagasse used in the simulation.

	Mass fraction (%)
Volatiles	40.88
Fixed carbon	8.24
Ash	0.88
Moisture	50.00

Table 5
Elemental analysis of the sugarcane bagasse used in the simulation.

	Mass fraction (%)
Carbon	42.84
Hydrogen	6.30
Oxygen	43.96
Nitrogen	6.90

Table 6
Mass flow and temperature of fuel and oxidant entering the boiler.

	Total mass flow (kg/s)	Inlets	Temperature (K)
Primary air	33.64	1	544.15
Secondary air	42.04	40	625.15
Pneumatic air	7.76	6	544.15
Biomass	22.63	6	300.00

The flow field was obtained by solving the conservation of momentum equations, and the turbulence modeling was done using the standard k-ε model. The effect of radiation was also considered in solving energy equation by taking the discrete ordinates (DO) model, which allows to include the effect of a discrete phase of particulate on radiation.

Given the large number of thermochemical processes happening on the grate and their importance on the overall combustion behavior in continuous phase, it is crucial to have an accurate grate model. In this study, the furnace grate consists of a set of 3348 (93×36) Pin Hole Continuous plates (PHC). Each plate has 12 holes of 7 mm in diameter, resulting in a stationary grate with total number of 40,176 holes. Due to the large number of holes, the discretization of the actual grate geometry in the furnace domain represents a major problem, leading to an excessive amount of computer memory needed to perform the computation. On the other hand, due to the important effect of these small holes on the primary air pressure drop, the removal of the grid from the computational domain is not a good option either and may result in unrealistic results and consequently large errors.

The pressure drop across perforated plates was predicted by Gan and Riffat [37] using CFD and the performance of this technique was validated by comparing their result against experimental data. A similar technique was used in this paper to set the viscous and inertial resistance coefficients of a porous medium considered as an equivalent to the furnace grate [38]. Table 1 shows the direction vectors and parameters describing the porous medium as explained in Eq. (1). In this table, direction 1 is a vector coax to the holes, while directions 2 and 3 are vectors perpendicular to direction 1.

$$S_i = -\left(\sum_{j=1}^{3} D_{ij}\mu v_j + \sum_{j=1}^{3} C_{ij}\frac{1}{2}\rho|v|v_j\right) \quad (1)$$

Eq. (1) represents the momentum source term from the porous medium where D_{ij} and C_{ij} are viscous and inertial resistance respectively, μ is the viscosity, ρ is the density and v the velocity of the fluid.

2.2. Modeling the discrete phase

A stream of biomass into a furnace could be considered as a group of particles with various sizes and shapes which result in different heat/mass interaction with the continuous phase. While the smaller particles are near spherical, the larger ones are mostly cylindrical and therefore a shape factor needs to be defined in order to approximate them to spherical particles [38]. To handle this and also in order to facilitate post-processing of the results, twelve different particle sizes were considered for each of the six biomass inlets. Immersed fuel particles travel through the continuous medium following a path governed by integrating forces balance on the particle. As the biomass particles travel through the hot gases, mass and heat exchange with the continuous phase is considered. These phenomena define the mass (species) and energy source terms for the conservation equations in the continuous phase. It is also worth mentioning that sugarcane bagasse is transported from the sugar mills to the boiler without any special processing and therefore is introduced to the furnace in wet from. To fully consider the heat and mass exchange phenomena, several processes need to be considered. In this study, inert heating/cooling, drying (either by evaporation or boiling), devolatilization (defined by a User-Defined Function), and finally combustion of carbon and inert heating/cooling of ashes were considered. If the conditions for a given particle are such that it reaches the surface of the grate, it will stay in that position, releasing its moisture and volatile content, releasing or absorbing energy via each of the above mentioned processes, and finally being fully depleted after releasing carbon dioxide and consuming oxygen due to the char combustion. All these processes on the grate were also programmed using a User-Defined Function.

Table 2 shows a summary of all the models used in the definition of both the continuous and the discrete phase. Details of UDFs as well as of used models can be found annexed to this paper as Supplementary Material [5,12,13,41–50].

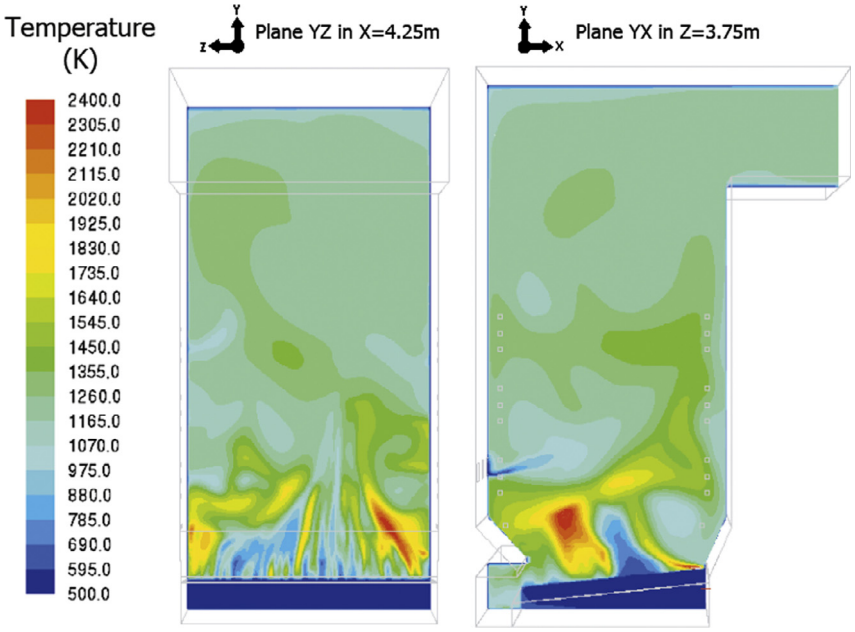

Fig. 3. Contours of temperature.

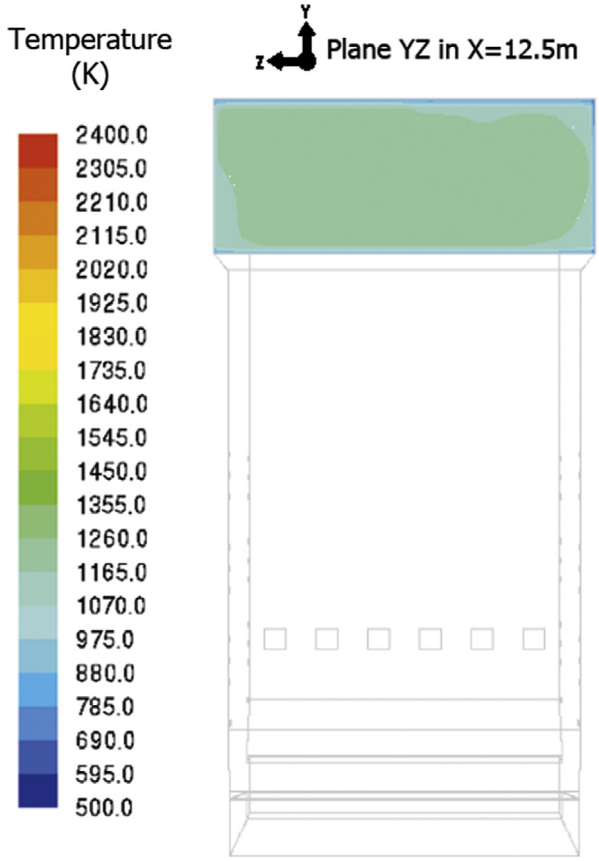

Fig. 4. Contour of the furnace outlet section temperature.

2.2.1. Devolatilization model

To set up the parameters of the biomass devolatilization model, samples of bagasse were first analyzed in a thermogravimetric analysis (TGA) system at three constant heating rates of 5, 10 and 15 °C/min. The circles in Fig. 1 show that the rate of conversion of biomass changes at conversion factor of around 0.6 and therefore the conversion process could be considered to mainly occur in two intervals. Ozawa, Flynn and Wall (OFW) method [39,40] was then employed to select the best reaction models that matches well with TGA data through all intervals of conversion fraction. Among 17 possible models tested against TGA data, a second order model for the first interval and a third order model for the second interval were selected to represent conversion of biomass through devolatilization process. The solid lines in Fig. 1 show these two models and how well they match with the TGA data. The activation energy and pre-exponential factors generated from OFW method for each model have also been listed in Table 3.

$$\frac{d\alpha}{dt} = A_i e^{\left(\frac{-E_{ai}}{RT_p}\right)} (1-\alpha)^2 \tag{2}$$

$$\frac{d\alpha}{dt} = A_i e^{\left(\frac{-E_{ai}}{RT_p}\right)} (1-\alpha)^3 \tag{3}$$

In Eqs. (2) and (3) α is the conversion fraction, t is the time, A_i is the pre-exponential factor, E_{ai} is the activation energy, R is the universal gas constant (8.314472 J/K mol), and T_p is the particle temperature.

3. Geometry

Fig. 2 shows the geometry of the boiler furnace which consists of the following main components:

- Six biomass inlets in the front wall, each equipped with a high pressure/velocity pneumatic air supply to give direction to the biomass stream upon injection.
- 40 Secondary air inlets distributed in 10 groups, each group located vertically along the edges of the side walls.
- A Pinhole Continuous (PHC) grate that distributes the primary air.
- The primary air inlet on the rear wall, just underneath the grate.
- The exhaust window at the top of the rear wall.

Further details of geometry and numerical mesh can be found as Supplementary Material.

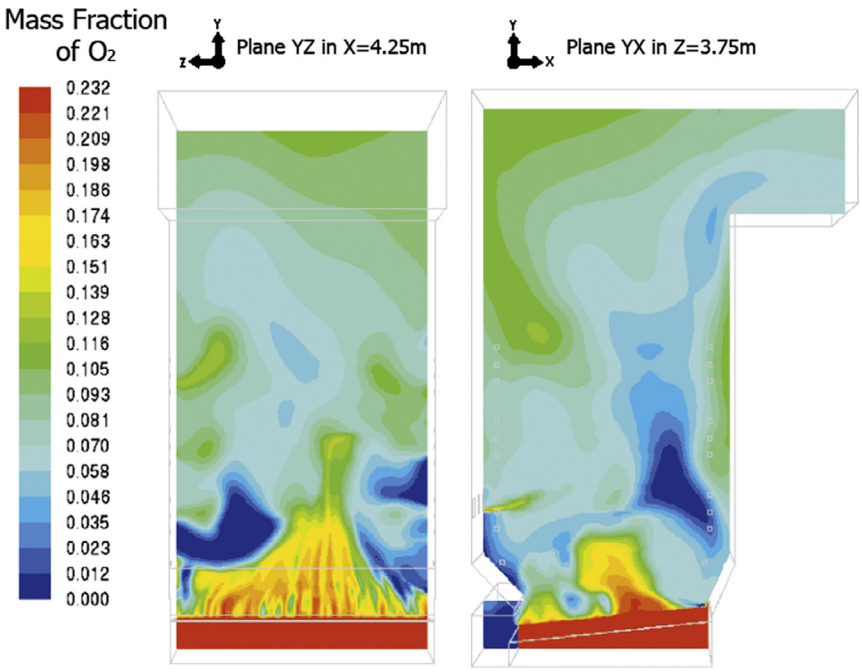

Fig. 5. Contours of oxygen mass fraction.

4. Setup and boundary conditions

Tables 4 and 5 show the proximate and elemental analysis respectively of the sugarcane bagasse used in the simulation. The higher calorific value of the biomass used in this study was also 8660.30 kJ/kg (as-received) and its dry density was 911.50 kg/m^3. Table 6 shows the input data for biomass and air.

Considering that all the steam tubes pass through the boiler walls, its temperature was considered to be the saturated steam temperature one at the drum pressure of 70.8 bar and equal to 559 K.

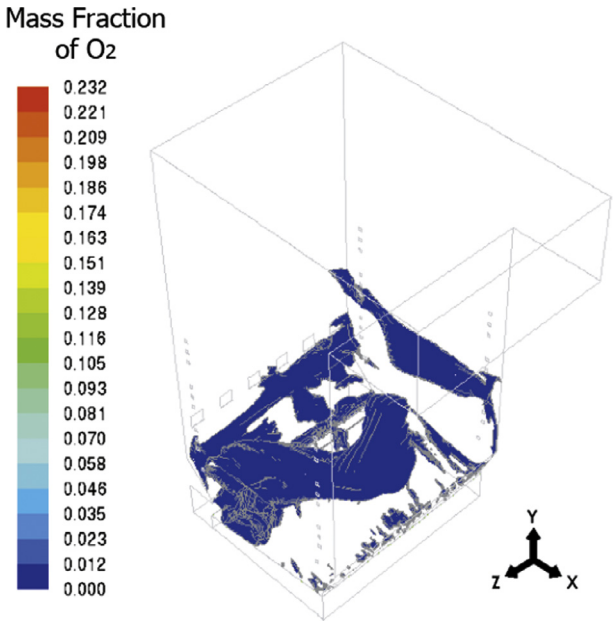

Fig. 6. Iso-surface illustrating regions where the mass fraction of oxygen (O_2) is close to zero.

For gas phase reaction, the following two-step mechanism was considered:

$$C_{0.78}H_{2.25}O_{0.99}N_{0.1775} + 0.45O_2 \rightarrow 0.78CO + 1.12H_2O + 0.0887N_2 \quad (4)$$

$$CO + 0.5O_2 \rightarrow CO_2 \quad (5)$$

where $C_{0.78}H_{2.25}O_{0.99}N_{0.1775}$ is the empirical formula of volatile fraction.

5. Results and discussions

Fig. 3 shows the temperature contours, in which a strong reaction zones is visible near to the grate. It is possible to observe that low temperature area on the grate perfectly match with regions of high oxygen content, and high temperature regions are just around, which characterize a diffusion flame having the oxidant inside. On the other hand Fig. 4 shows the contours of the furnace outlet section temperature where the average temperature of around 900 °C is in agreement with the manufacturer reported measurements.

Contours of Oxygen mass fraction (O_2) have been shown in Fig. 5. The left image in this figure clearly displays how the non-premixed flame shape is developed and emerged from the grate. The oxygen-scarce regions could also be tracked by looking at areas in blue; however, this can be best visualized using the iso-surface shown in Fig. 6. This iso-surface could be used to locate the areas that might need a better distribution of secondary air in order to improve combustion.

Fig. 7 shows the particles' trajectories colored by the current heat and mass transfer processes occurring between the particle and the continuous phase. As mentioned in Section 2.2, twelve streams of biomass particles were considered for each biomass inlet in order to represent the wide range of particle sizes. These injection streams which have been numbered from 00 to 11 represent particle sizes in an ascending order of size with Injection 00 as the smallest and Injection 11 as the largest group of particles. The

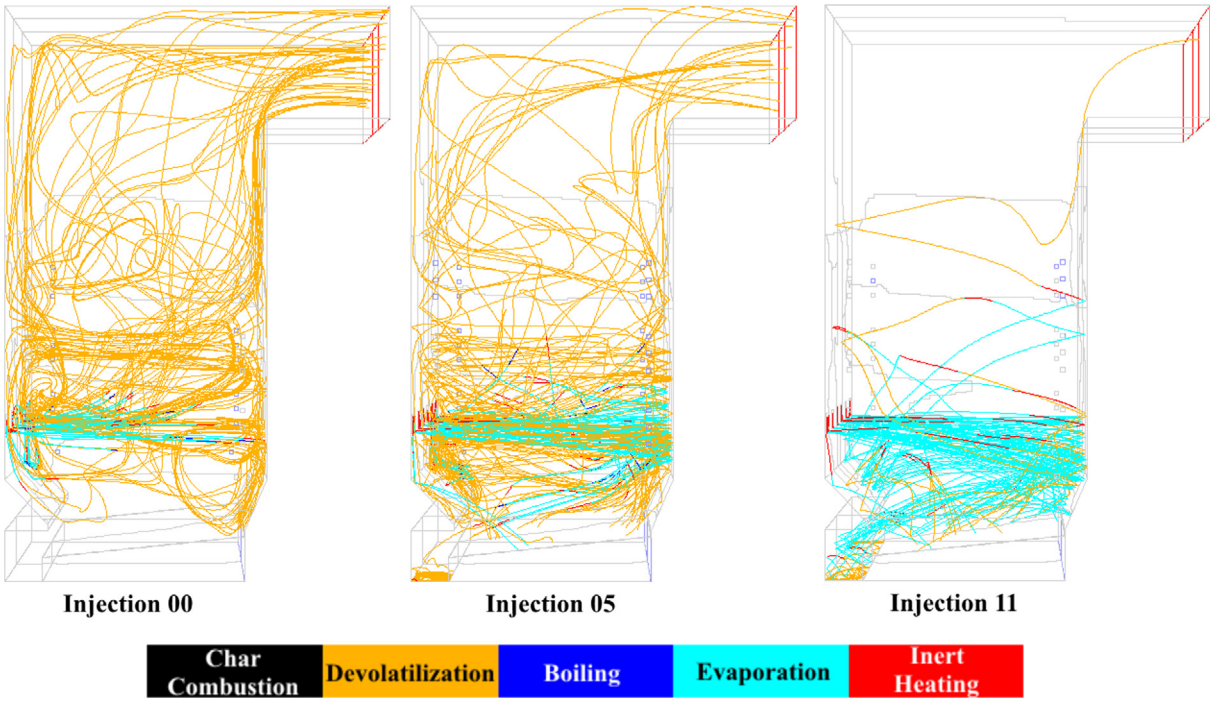

Fig. 7. Trajectories of biomass particles colored by heat and mass transfer processes. The particle size increases from Injection 00 to 11 as shown in Table 5.

Table 7
Content of particles per injection.

Injection	Equivalent diameter (mm)	Mass flow (kg/s)	Moisture			Volatiles			Char		
			Total (kg/s)	Grate (%)	Exit (%)	Total (kg/s)	Grate (%)	Exit (%)	Total (kg/s)	Grate (%)	Exit (%)
00	0.38	0.34	0.17	0.00	0.00	0.14	2.48	4.74	0.03	11.67	88.33
01	0.48	1.34	0.67	0.00	0.00	0.55	5.16	4.75	0.11	15.00	85.00
02	0.54	2.94	1.47	0.00	0.00	1.20	4.04	4.44	0.24	11.66	86.67
03	0.68	6.38	3.19	0.00	0.00	2.61	11.12	3.40	0.53	30.00	70.00
04	0.76	2.09	1.04	0.00	0.00	0.85	4.43	3.40	0.17	21.67	76.66
05	0.96	1.54	0.77	0.61	0.00	0.63	18.82	1.54	0.13	58.34	35.00
06	1.08	3.55	1.77	0.28	0.00	1.45	27.30	1.10	0.29	60.00	23.33
07	1.21	2.04	1.02	2.03	0.00	0.83	37.30	0.25	0.17	73.33	5.00
08	1.34	1.21	0.60	7.37	0.00	0.49	53.91	0.20	0.10	83.33	5.00
09	1.53	0.79	0.40	15.62	0.00	0.32	72.90	0.16	0.07	93.33	3.33
10	1.68	0.23	0.12	25.00	0.00	0.09	76.75	0.16	0.02	93.33	3.33
11	1.78	0.19	0.09	23.50	0.00	0.08	86.60	0.11	0.02	96.67	1.67

Table 8
Gas flow at the furnace exit.

Vol (g/s)	O_2 (kg/s)	CO_2 (kg/s)	H_2O (kg/s)	CO (g/s)	N_2 (kg/s)
5.37	7.77	15.27	18.37	4.19	63.28

detail information regarding each injection have been presented in Table 7.

From the colored trajectories in Fig. 7, it could be deduced that in general the drying process takes place at the lower zones of furnace and mainly due to vaporization. However, the volatilization seems to be completely distributed all over the furnace and take place throughout all zones. In terms of char combustion, it is difficult to observe it anywhere along the trajectories. This suggests that based on the initial size of the biomass particles, the char either burns on the grate or is dragged to the exit of the furnace. Therefore, it could be concluded that larger particles tend to burn on the grate while the smaller ones tend to follow the flow and burn within the furnace and leave the boiler as char. In that sense, having larger particles seems to yield a more complete and hence a more efficient combustion. On the other hand, larger particle are more likely to reach the rear wall and increase the possibility of slagging. Fig. 7 only shows an illustration of three streams representing small, medium and large size particles. The complete information of all injections including their size distribution and fraction of processes occurring on the grate and exit flow have been presented in Table 7.

The result from CFD analysis could also be used to calculate the "overall efficiency" of the combustion using Eq. (6):

$$\eta = 100 - q_{gas} - q_{solid} \tag{6}$$

In this equation q_{gas} and q_{solid} are indicators of energy loss from unburned gases and solids respectively. From the data in Table 7

and using the following Eq. (7) the contribution of unburned solids in dropping overall efficiency is found to be 20.38%:

$$q_{solid} = \frac{100(\dot{m}_{vol\_s} LHV_{vol} + \dot{m}_{C} LHV_{C})}{\dot{m}_{biom} LHV_{biom} + \sum_{i=1}^{3} \dot{m}_{air_i} (h_{air_i@T_i} - h_{air_i@T_0})} \quad (7)$$

In Eq. (7) $\dot{m}_{vol\_s}$ and $\dot{m}_{C}$ are respectively mass flow of volatile and fixed carbon not released from the particles leaving the furnace, $\dot{m}_{biom}$ and $\dot{m}_{air}$ are respectively mass flow of total biomass and air coming into the furnace, LHV_{vol}, LHV_{C} and LHV_{biom} are respectively lower heating value of volatiles, carbon and the biomass, $h_{air_i@T_i}$ and $h_{air_i@T_0}$ are respectively enthalpies of air at inlet temperature and at ambient temperature. Finally, the sum in the denominator of Eq. (7) is made on each of the three types of air inlets (primary, secondary and pneumatic).

To find q_{gas} the composition of gases at the furnace exit is required. Using this data summarized in Table 8 and from equation (8) it was found that unburned gases have a minimal impact and result in only 0.07% reduction of overall efficiency.

$$q_{gas} = \frac{100(\dot{m}_{vol\_g} LHV_{vol} + \dot{m}_{CO} LHV_{CO})}{\dot{m}_{biom} LHV_{biom} + \sum_{i=1}^{3} \dot{m}_{air_i} (h_{air_i@T_i} - h_{air_i@T_0})} \quad (8)$$

In Eq. (8) $\dot{m}_{vol\_g}$ and $\dot{m}_{CO}$ are respectively mass flow of volatiles and carbon monoxide into the exhaust gases, LHV_{vol} and LHV_{CO} are respectively lower heating value of volatiles and carbon monoxide and finally the denominator is the same with Eq. (7).

Finally and as it was explained in Eq. (6), the overall efficiency of the combustion in this case was calculated to be 80%.

It is worth to mention that the data in Table 7 would not be easy to be obtained from experimental measurements; therefore the so-called "overall efficiency" obtained from CFD analysis could be considered as an important indicator that could allow comparing different design scenarios and operational alternatives, even if absolute values could not be real.

6. Conclusions

In this study, CFD analysis was employed to model the combustion of sugarcane bagasse in an industrial boiler. Biomass was considered as a discrete phase and its interaction with the continuous gas phase was modeled using ANSYS Fluent built-in functions as well as in house UDF codes. The simulation provided a clear understanding of phenomena that a single biomass particle goes through from initial heating all the way to char combustion and its conversion to ash. It was shown that larger particles are more likely to burn to completion on the grate and it than sense having a knowledge on the initial size distribution of biomass fuel is crucial to have an efficient combustion. The simulation also helped to have a better understanding of both volatile and oxygen distribution across different regions within the boiler. Devolatilization is specifically important because it will help us to predict thermal field and eventually improve boiler efficiency. Knowledge on oxygen-scarce zones could also help operators to adjust airflow and injection angle in order to improve combustion. The CFD analysis in this work was also used to find the overall efficiency. Such analysis could be used as an inexpensive measure to try different design parameters and understand their impact on boiler performance before taking any costly step in practice.

Acknowledgments

The authors would like to thank the financial support in the form of scholarship from CAPES, CNPq, PRH-16 ANP and FAPEMIG of Brazil and the financial support of the CNPq process 407050/2013-2. It is also important to acknowledge the support of boiler manufacturer Caldema Equipamentos Industriais Ltda.

Appendix A. Supplementary material

Supplementary data associated with this article can be found, in the online version, at http://dx.doi.org/10.1016/j.fuel.2016.11.105.

References

[1] Demirbas A. Potential applications of renewable energy sources, biomass combustion problems in boiler power systems and combustion related environmental issues. Prog. Energy Combust. Sci. 2005;31:171–92.
[2] Belosevic S. Modeling approaches to predict biomass co-firing with pulverized coal. Open Thermodyn J 2010;4.
[3] Bharadwaj A, Baxter LL, Robinson AL. Effects of intraparticle heat and mass transfer on biomass devolatilization: experimental results and model predictions. Energy Fuels 2004;18:1021–31.
[4] Baxter L. Biomass-coal co-combustion: opportunity for affordable renewable energy. Fuel 2005;84:1295–302.
[5] Boyd RK, Kent JH. Three-dimensional furnace computer modelling. Symp (Int) Combust 1988;21:265–74.
[6] Woodfield PL, Kent JH, Dixon TF. Computational modelling of combustion instability in bagasse-fired furnaces. Exp Therm Fluid Sci 2000;21:17–25.
[7] Woodfield PL, Kent JH, Dixon TF. Temperature measurements in a bagasse-fired furnace-experimental and numerical results. In: Proceedings of australian society of sugar cane technologists, 1997. p. 473–478.
[8] Woodfield PL, Kent H, Dixon TF. Computational modelling of a bagasse-fired furnace. Effects of fuel moisture. In: Proceedings of the Australian society of sugar cane technologists (ASSCT), Australia. 1998. p. 458–64.
[9] Stastny M, Ahnert F, Spliethoff H. Three-dimensional combustion modelling of a biomass fired pulverized fuel boiler. Heat Transfer 2002;2002:119–26.
[10] Gera D, Mathur MP, Freeman MC, Robinson A. Effect of large aspect ratio of biomass particles on carbon burnout in a utility boiler. Energy Fuels 2002;16:1523–32.
[11] Sheng C, Moghtaderi B, Gupta R, Wall TF. A computational fluid dynamics based study of the combustion characteristics of coal blends in pulverised coal-fired furnace. Fuel 2004;83:1543–52.
[12] Zahirovic S, Scharler R, Obernberger I. Advanced CFD modelling of pulverised biomass combustion. In: International conference on science in thermal and chemical biomass conversion, Victoria, Canada. 2004.
[13] Backreedy RI, Fletcher LM, Jones JM, Ma L, Pourkashanian M, Williams A. Co-firing pulverised coal and biomass: a modeling approach. Proc Combust Inst 2005;30:2955–64.
[14] Rogerson JW, Kent JH, Bilger RW. Conditional moment closure in a bagasse-fired boiler. Proc Combust Inst 2007;31:2805–11.
[15] Ma L, Jones JM, Pourkashanian M, Williams A. Modelling the combustion of pulverized biomass in an industrial combustion test furnace. Fuel 2007;86:1959–65.
[16] Shanmukharadhya K, Sudhakar K. Experimental investigations for the location of reaction zones in a bagasse fired furnace. J Therm Anal Calorim 2007;90:299–306.
[17] Shanmukharadhya KS. Simulation and thermal analysis of the effect of fuel size on combustion in an industrial biomass furnace. Energy Fuels 2007;21:1895–900.
[18] Shanmukharadhya KS, Ramachandran K. Numerical and experimental investigations for optimisation of plant capacity for bagasse fired furnace. J Energy Inst 2009;82:69–75.
[19] Shanmukharadhya KS, Sudhakar KG. Effect of fuel moisture on combustion in a bagasse fired furnace. J Energy Res Technol 2006;129:248–53.
[20] Shanmukharadhya KS, Sudhakar KG. Investigations of effect of bagasse pyrolysis kinetics on combustion and boiler performance. J Energy Inst 2007;80:40–5.
[21] Ma L, Gharebaghi M, Porter R, Pourkashanian M, Jones JM, Williams A. Modelling methods for co-fired pulverised fuel furnaces. Fuel 2009;88:2448–54.
[22] Gubba SR, Ingham DB, Larsen KJ, Ma L, Pourkashanian M, Tan HZ, et al. Numerical modelling of the co-firing of pulverised coal and straw in a 300 MWe tangentially fired boiler. Fuel Process Technol 2012;104:181–8.
[23] Smith JD. Foundations of a three-dimensional model for predicting coal combustion characteristics in industrial power generation plants. In: Dept of Chemical Engineering. Provo, Utah, USA: Brigham Young University; 1990.
[24] Eastwick CN, Pickering SJ, Aroussi A. Comparisons of two commercial computational fluid dynamics codes in modelling pulverised coal combustion for a 2.5 MW burner. Appl Math Model 1999;23:437–46.
[25] FAO. Countries by commodity; 2012.
[26] Garzón-Barrero NM, Shirakawa MA, Brazolin S, de Barros Pereira RGdFN, de Lara IAR, Savastano Jr H. Evaluation of mold growth on sugarcane bagasse particleboards in natural exposure and in accelerated test. Int Biodeterior Biodegrad 2016;115:266–76.
[27] Goldemberg J. The Brazilian biofuels industry. Biotechnol Biofuels 2008;1:1–7.
[28] Beeharry RP. Extended sugarcane biomass utilisation for exportable electricity production in Mauritius. Biomass Bioenergy 1996;11:441–9.
[29] Kaltschmitt M, Reinhardt GA, Stelzer T. Life cycle analysis of biofuels under different environmental aspects. Biomass Bioenergy 1997;12:121–34.
[30] Schlamadinger B, Apps M, Bohlin F, Gustavsson L, Jungmeier G, Marland G, et al. Towards a standard methodology for greenhouse gas balances of

bioenergy systems in comparison with fossil energy systems. Biomass Bioenergy 1997;13:359–75.
[31] Brentrup F, Küsters J, Kuhlmann H, Lammel J. Application of the life cycle assessment methodology to agricultural production: an example of sugar beet production with different forms of nitrogen fertilisers. Eur J Agron 2001;14:221–33.
[32] Botha T, von Blottnitz H. A comparison of the environmental benefits of bagasse-derived electricity and fuel ethanol on a life-cycle basis. Energy Policy 2006;34:2654–61.
[33] Boog EG, Cidiki MC, Bizzo WA, de cana-de-açúcar Resíduos agrícolas. Novas perspectivas para geração de energia elétrica no estado de São Paulo. In: Pantano Filho R, Rosa DDS, editors. Desenvolvimento sustentável. Itativa, SP, Brasil: Berto editora; 2008.
[34] Kiatkittipong W, Wongsuchoto P, Pavasant P. Life cycle assessment of bagasse waste management options. Waste Manage 2009;29:1628–33.
[35] Chauhan MK, Varun S, Chaudhary S, Kumar Samar. Life cycle assessment of sugar industry: a review. Renew Sustain Energy Rev 2011;15:3445–53.
[36] Dantas GA, Legey LFL, Mazzone A. Energy from sugarcane bagasse in Brazil: an assessment of the productivity and cost of different technological routes. Renew Sustain Energy Rev 2013;21:356–64.
[37] Gan G, Riffat SB. Pressure loss characteristics of orifice and perforated plates. Exp Therm Fluid Sci 1997;14:160–5.
[38] Centeno González FO. Avaliação da Combustão de Bagaço e Palha de Cana-de-Açucar numa Fornalha de Caldeira Industrial AMD a partir da Modelagem por CFD. Itajubá, MG, Brasil: Instituto de Engenharia Mecânica, Universidade Federal de Itajubá; 2015. p. 162.
[39] Ozawa T. A new method of analyzing thermogravimetric data. Bull Chem Soc Jpn 1965;38:1881–6.
[40] Flynn JH, Wall LA. A quick, direct method for the determination of activation energy from thermogravimetric data. J Polym Sci C: Polym Lett 1966;4:323–8.
[41] Coppalle A, Vervisch P. The total emissivities of high-temperature flames. Combust Flame 1983;49:101–8.
[42] Smith TF, Shen ZF, Friedman JN. Evaluation of coefficients for the weighted sum of gray gases model. J Heat Transfer 1982;104:602–8.
[43] Magnussen BF, Hjertager BH. On mathematical modeling of turbulent combustion with special emphasis on soot formation and combustion. Symp (Int) Combust 1977;16:719–29.
[44] Spalding DB. Mixing and chemical reaction in steady confined turbulent flames. Symp (Int) Combust 1971;13:649–57.
[45] Miller RS, Harstad K, Bellan J. Evaluation of equilibrium and non-equilibrium evaporation models for many-droplet gas-liquid flow simulations. Int J Multiph Flow 1998;24:1025–55.
[46] Sazhin SS. Advanced models of fuel droplet heating and evaporation. Prog Energy Combust Sci 2006;32:162–214.
[47] Baum MM, Street PJ. Predicting the combustion behaviour of coal particles. Combust Sci Technol 1971;3:231–43.
[48] Field MA. Rate of combustion of size-graded fractions of char from a low-rank coal between 1200 K and 2000 K. Combust Flame 1969;13:237–52.
[49] Luo M, Stanmore B. The combustion characteristics of char from pulverized bagasse. Fuel 1992;71:1074–6.
[50] Agraniotis M, Nikolopoulos N, Nikolopoulos A, Grammelis P, Kakaras E. Numerical investigation of solid recovered fuels' co-firing with brown coal in large scale boilers – evaluation of different co-combustion modes. Fuel 2010;89:3693–709.